A calcium-influx-dependent plasticity model exhibiting multiple STDP curves

Akke Mats Houben[1] · Matthias S. Keil[1]

Abstract

Hebbian plasticity means that if the firing of two neurons is correlated, then their connection is strengthened. Conversely, uncorrelated firing causes a decrease in synaptic strength. Spike-timing-dependent plasticity (STDP) represents one instantiation of Hebbian plasticity. Under STDP, synaptic changes depend on the relative timing of the pre- and post-synaptic firing. By inducing pre- and post-synaptic firing at different relative times the STDP curves of many neurons have been determined, and it has been found that there are different curves for different neuron types or synaptic sites. Biophysically, strengthening (*long-term potentiation*, LTP) or weakening (*long-term depression*, LTD) of glutamatergic synapses depends on the post-synaptic influx of calcium (Ca^{2+}): weak influx leads to LTD, while strong, transient influx causes LTP. The voltage-dependent NMDA receptors are the main source of Ca^{2+} influx, but they will only open if a post-synaptic depolarisation coincides with pre-synaptic neurotransmitter release. Here we present a computational mechanism for Ca^{2+}-dependent plasticity in which the interplay between the pre-synaptic neurotransmitter release and the post-synaptic membrane potential leads to distinct Ca^{2+} time-courses, which in turn lead to the change in synaptic strength. It is shown that the model complies with classic STDP results, as well as with results obtained with triplets of spikes. Furthermore, the model is capable of displaying different shapes of STDP curves, as observed in different experimental studies.

Keywords Synaptic plasticity · STDP · Calcium-dependent-plasticity

1 Introduction

Synaptic plasticity is a mechanism for storing information in the brain, and determines the organisation and communication of neurons after their initial development. Thus it is an important factor to investigate to understand information processing in the nervous system. An initial conceptual description of synaptic plasticity has been famously proposed by Hebb (1949) which boils down to the idea that correlated activity of two neurons leads to a strengthening, or *long-term potentiation* (LTP), of the connection between them (Hebb 1949). Although Hebb did not postulate any mechanism for synaptic weakening (*long-term depression*, LTD), most implementations combine a LTP mechanism with a complementary LTD mechanism to prevent the synaptic weights from saturating and to implement a form of competition (Song et al. 2000).

The translation of this conceptual description to actual implementations which can be modelled and tested has taken on different forms. Experiments indicated an important role for the *relative* timing of pre- versus post-synaptic spikes: firing of the pre-synaptic neuron before the post-synaptic neuron (*pre-post* pairing) leads to LTP, whereas post-synaptic firing before pre-synaptic firing (*post-pre* pairing) leads to LTD (Markram et al. 1997; Bi and Poo 1998), which confirmed a computational model proposed earlier (Gerstner et al. 1996). This has lead to the most widely used phenomenological model for synaptic plasticity: *spike-timing-dependent plasticity* (STDP) (Song et al. 2000). This has later been extended to account for synaptic changes following more complex pre- and post-synaptic spiking patterns (Froemke and Dan 2002; Froemke et al. 2006; Pfister and Gerstner 2006). Figure 1 shows the classic STDP curve (adapted from Song et al. 2000), which has been derived from experimental observations in which

✉ Akke Mats Houben
akkehouben@gmail.com

1 Institute of Neurosciences and Faculty for Psychology, University of Barcelona, Passeig de la Vall d'Hebron 171, 08035 Barcelona, Spain

Fig. 1 Classic STDP curve as described by Song et al. (2000), with a LTP window for *pre-post* ($\Delta t < 0$) firing and a LTD window for *post-pre* ($\Delta t > 0$) firing
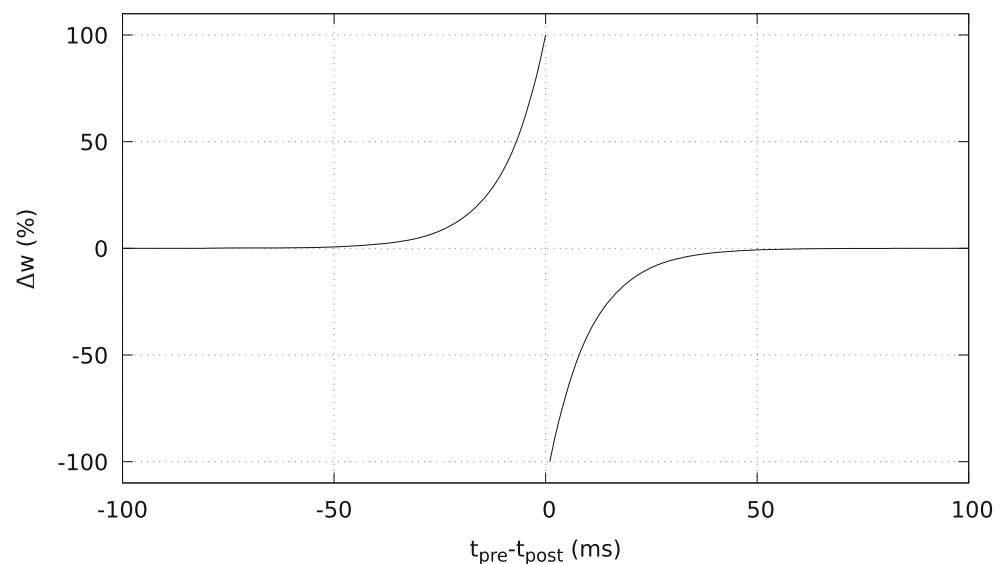
the synaptic changes have been measured after many spike-pairings.

Nevertheless, many different types of synapses exist, which exhibit different changes in synaptic weights, depending on the relative pre- and post-synaptic spike timings. Examples of these different STDP windows are: anti-Hebbian plasticity (Fig. 2a), LTD biased (Fig. 2b), uni-directional STDP expressing only LTP or LTD in half of the classical STDP window (Fig. 2c to f) or STDP windows in which all relative spike-timings result in either LTP or LTD (Fig. 2g and h). The difference in shapes depend on the neuron types involved (Tzounopoulos et al. 2004; Lu et al. 2007; Fino et al. 2008), the location of the synapse on the dendrite (Froemke et al. 2005; Letzkus et al. 2006; Sjöström and Häusser 2006) and the active properties of the dendrite (Sourdet and Debanne 1999).

1.1 Biophysical mechanisms of STDP

Early on it was understood that, for glutamatergic synapses, the main component of synaptic plasticity was mediated by calcium (Ca^{2+}) influx into the post-synaptic cell (Malenka et al. 1988; Lisman 1989), through the activation of post-synaptic NMDA receptors by pre-synaptically released glutamate (Bi and Poo 1998; Yang et al. 1999). LTP is induced by a transient, high magnitude increase of Ca^{2+}, whereas LTD results from more prolonged, modest Ca^{2+} levels (Yang et al. 1999; Abbott and Nelson 2000; Graupner and Brunel 2010). The synaptic weights are altered by Ca^{2+}-dependent alteration of AMPA receptor number or efficacy (Malinow and Malenka 2002; Graupner and Brunel 2007). A high rise in Ca^{2+} results in calcium/calmodulin-dependent protein kinase II (CaMKII) which leads to a phosphorylation of AMPA receptors (Malenka et al. 1989;

Holmes 2000; Colbran 2004; Wang et al. 2005; Lisman et al. 2012), leading to LTP. Lower Ca^{2+} influx results in calcineurin (CaN) activation, leading to dephosphorylation of AMPA receptors, which results in LTD (Lisman 1989; Colbran 2004; Wang et al. 2005).

NMDA receptors are blocked by magnesium (Mg^{2+}) at resting potential and an increase (depolarisation) of the (local) membrane potential is needed for Mg^{2+} to be repelled from the NMDA receptors (Jahr and Stevens 1990; Dayan and Abbott 2001). Post-synaptic firing causes the propagation of an action potential down the axon and a backpropagation of the action potential up the dendrites. This *backpropagating action potential* links the post-synaptic response to previously activated synapses, by depolarising the dendritic spine (the post-synaptic side of the synapse) and in this way opening the NMDA receptors for Ca^{2+} influx. This mechanism can be seen as a coincidence detector: in order for NMDA receptors to allow an influx of Ca^{2+}, a co-occurrence of pre-synaptic activity, leading to neurotransmitter release, and a post-synaptic depolarisation, to relieve the Mg^{2+} block of the NMDA receptors, is needed.

1.2 Models of Ca^{2+}-mediated plasticity

Following the possibility of NMDA receptor-dependent Ca^{2+} influx to act as an coincidence detector, several studies have modelled synaptic plasticity following the above mentioned Ca^{2+} influx mechanism in order to account for the spike-timing-dependence of STDP. The first set of models test the *calcium control hypothesis*, which states that synaptic modification occurs when the intra-cellular Ca^{2+} concentration $[Ca^{2+}]$ is above some threshold. Above this threshold two regions exist:

(a) anti-Hebbian

(b) LTD biased

(c) pre-LTP

(d) pre-LTD

(e) post-LTP

(f) post-LTD
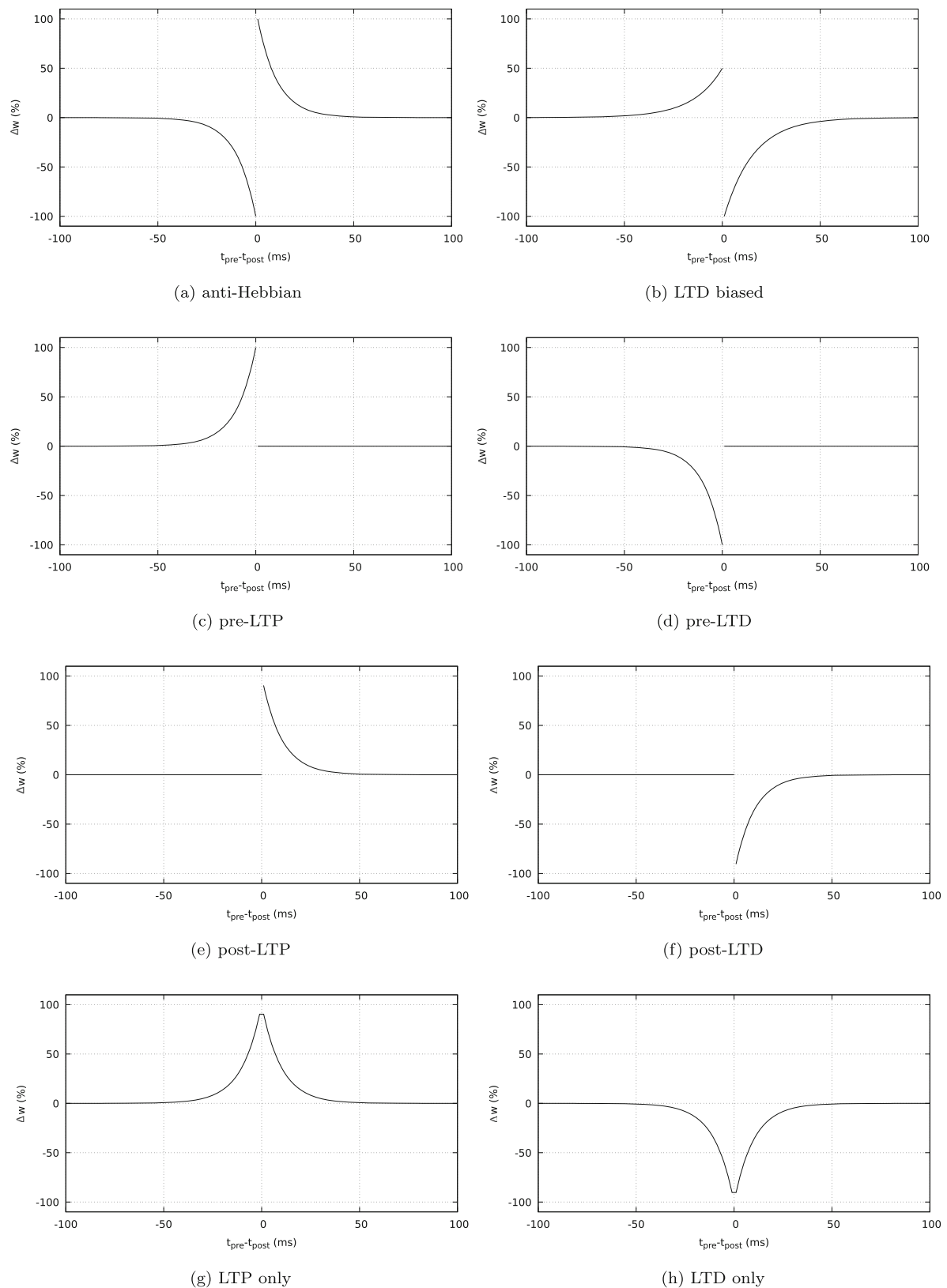
(g) LTP only

(h) LTD only

Fig. 2 Different STDP curves as found for different synapses. **a** anti-Hebbian: a LTD window for $\Delta t < 0$ and LTP for $\Delta t > 0$; **b** LTD biased: a bigger LTD window than LTP window; **c** pre-LTP: only a LTP window for $\Delta t < 0$; **d** pre-LTD: only a LTD window for $\Delta t < 0$; **e** post-LTP: same as (**c**), but for $\Delta t > 0$; **f** post-LTD: same as (**d**), but for $\Delta t > 0$; **g** LTP only: a symmetric window with only LTP; **h** LTD only: same as (**g**), but only LTD

intermediate $[Ca^{2+}]$ levels result in LTD and $[Ca^{2+}]$ levels above a second threshold trigger LTP (Shouval et al. 2002; Cai et al. 2007; Graupner and Brunel 2010). In order to differentiate the $[Ca^{2+}]$ levels resulting from *pre-post* pairing from those resulting from *post-pre* pairing, a long after-depolarisation after the post-synaptic spike is needed. The predictions of these models reach a high level of agreement with experimental results, yet predict also an additional LTD region for *pre-post* pairing which is not observed in most STDP experiments (Gerkin et al. 2010; Graupner and Brunel 2010), and seems an inevitable consequence of using only post-synaptic $[Ca^{2+}]$ levels as a signal for synaptic plasticity (Rubin et al. 2005; Gerkin et al. 2010). By adding stochastic synaptic transmission the *pre-post* LTD window can be reduced (Shouval and Kalantzis 2005). The model of Cai et al. (2007) extends the calcium control model in order to account for multi-spike STDP results. Abarbanel et al. (2003) use a non-linear competition between two signals derived from the calcium time-course. Yet the main factor determining synaptic plasticity is the amplitude of the Ca^{2+}-influx (Abarbanel et al. 2003), making the results similar to those of other calcium control hypothesis models (Graupner and Brunel 2010).

The *pre-post* and *post-pre* pairing Ca^{2+} signals differ in more than just the peak or mean $[Ca^{2+}]$ levels they result in (Mizuno et al. 2001; Graupner and Brunel 2010), moreover the values of $[Ca^{2+}]$ seem to be uncorrelated with the direction of synaptic change (Nevian and Sakmann 2006). According to the calcium control hypothesis, large and transient Ca^{2+}-influx leads to LTP and persistent, low Ca^{2+}-influx leads to LTD. Thus, besides the absolute Ca^{2+} levels, there is an importance of the time window (or time course) in which the Ca^{2+} influx occurs for determining LTP and LTD (Sjöström and Nelson 2002). The model proposed by Rubin et al. (2005) uses three signals derived from the Ca^{2+}-influx, which provide a mechanism that represents the CaMKII AMPA phosphorylation (Rubin et al. 2005; Graupner and Brunel 2010). A transient, high $[Ca^{2+}]$ level activates a signal that promotes LTP. Another signal builds up slowly in response to slow and prolonged $[Ca^{2+}]$ elevations and leads to LTD. A "veto" mechanism is activated rapidly at intermediate $[Ca^{2+}]$ levels, which inhibits LTD (Rubin et al. 2005). The study of Gerkin et al. (2010) builds further upon this model. A similar model is that of Kubota and Kitajima (2008). This model uses both the peak $[Ca^{2+}]$ levels aswell as the time that the $[Ca^{2+}]$ spends above a certain threshold to determine the synaptic change.

The work of Graupner and Brunel (2007) and Urakubo et al. (2008) describe the connection between the $[Ca^{2+}]$ levels and the phosphorylation level of the CaMKII protein (Graupner and Brunel 2007; Urakubo et al. 2008; Graupner and Brunel 2010). In both models LTP is induced by

fast and high Ca^{2+} transients and LTD is induced by intermediate $[Ca^{2+}]$ levels. The models differ however in the specific mechanisms used to obtain the STDP curve (Graupner and Brunel 2010): Urakubo et al. (2008) propose time-difference-sensitive allosteric kinetics of the NMDA receptors to predict the STDP curve. They propose spike-timing dependent suppression of NMDA receptors by Ca^{2+}-calmodulin in which *pre-post* pairing leads to a slow suppression and *post-pre* pairing to a fast suppression (Urakubo et al. 2008). The model of Graupner and Brunel (2007) suggest that the stronger activation of a LTP inducing pathway, due to higher $[Ca^{2+}]$ levels for *pre-post* pairing, acts like a "veto" that inhibits the LTD induced by intermediate $[Ca^{2+}]$ levels (Graupner and Brunel 2007; 2010).

Other models incorporate distinct 'pathways' for LTD and LTP (Karmarkar and Buonomano 2002; Badoual et al. 2006; Carlson and Giordano 2011). In the model of Karmarkar and Buonomano (2002) LTP follows from glutamatergic activation of NMDA receptors and the subsequent Ca^{2+}-influx through them, where LTD results from Ca^{2+}-influx through voltage-gated calcium channels co-occurring with glutamatergic activation of metabotropic glutamate receptors (mGluR). Yet the involvement of mGluRs in the induction of LTD is debated due to its slow activation (Badoual et al. 2006). The model of Badoual et al. (2006) uses two coincidence detectors: one sensitive to Ca^{2+}, and the other to glutamate. The model describes two abstract enzymes of which one, only sensitive to Ca^{2+}, results in LTP and the other, which uses both Ca^{2+} and glutamate, to LTD. The model of Carlson and Giordano (2011) utilises both the NMDA receptors as well as voltage gated calcium channels to model the Ca^{2+} dynamics needed for STDP.

For a review of models and proposed STDP mechanisms in biophysical models see Graupner and Brunel (2010).

The current study extends previous efforts to model the underlying mechanisms of STDP by modelling the interplay of the post-synaptic membrane potential and neurotransmitter release, and their effects on the Ca^{2+} influx through the NMDA receptors, which in turn determines the synaptic change. Here we develop a model of the mechanisms underlying plasticity in glutamatergic synapses in which the synaptic Ca^{2+} dynamics are explicitly linked to the membrane potential V_m of the model neuron. The model captures the influence of the neurotransmitter release on the membrane potential and the reciprocal effect of the membrane potential on the efficacy of the neurotransmitter. This interplay, and the resulting Ca^{2+} dynamics, leads to a model that captures classical STDP results, but also complies with extensions of the classical STDP curve: it is able to comply with triplet STDP experiments (Froemke and Dan 2002; Froemke

et al. 2006; Pfister and Gerstner 2006), and is capable of exhibiting different STDP curves, as found in biological neurons (Froemke et al. 2005; Letzkus et al. 2006; Lu et al. 2007; Fino et al. 2008), by the alteration of two parameters. Crucially, the model explores the question of synaptic change taking two important discrepancies between experimental observations and the hypothesis that synaptic plasticity follows from (solely) the maximal or average Ca^{2+} levels. The two observations taken into account are: 1) Ca^{2+} concentrations are unrelated to the synaptic change (Nevian and Sakmann 2006) and 2) that the time-course of the Ca^{2+} influx also carries information on the order of spike occurence (Mizuno et al. 2001; Sjöström and Nelson 2002).

2 Methods

The post-synaptic neuron is modelled as a simple leaky integrate-and-fire neuron, with a membrane equation (adapted from Dayan and Abbott 2001) that includes two additional currents for the AMPA and NMDA receptors:

$$\tau_m \frac{dV}{dt} = I - g_L(V - E_L) - g_{ampa}(V - E_{ampa})$$
$$- g_{nmda}(V - E_{nmda}) \qquad (1)$$

With auxiliary reset rule: $V > E_{th} \implies V \leftarrow E_{reset}$ accounting for spiking behavior. The AMPA and NMDA currents will be defined in the following sections.

Even though the neuron is modelled as a single compartment, the Ca^{2+} currents resulting in the synaptic plasticity need to be calculated for each synapse independently. As a consequence also the variables that govern the Ca^{2+} currents need to be determined for each synapse. One of the two main events involved in STDP is the post-synaptic action potential (AP), which causes a depolarisation of the membrane potential that expels the Mg^{2+} from the NMDA receptors and thus allows Ca^{2+} influx through these NMDA receptors. Even though dendrites can actively propagate APs, the magnitude decreases and width increases with distance traveled (Waters et al. 2005; Feldman 2012), effectively functioning as a low-pass filter. Therefore, for the calculation of the synapse-specific Ca^{2+} current, a low-pass filtered version of the membrane potential V_i is used, per synapse i:

$$\tau_V \frac{dV_i}{dt} = -V_i + V \qquad (2)$$

In which τ_V is the time constant of the dendritic membrane potential. The low-pass filtered version of the membrane potential is a coarse approximation of the effect of distance from the point of AP initiation, yet it will serve well as a first approximation. As will be shown later, different values for τ_V will result in different STDP curves.

2.1 NMDA Ca^{2+} current

The Ca^{2+} current, as calculated per synapse i, is derived from a part of the membrane equation:

$$I_{Ca^{2+}} = (1 - [Ca^{2+}])g_{nmda}(V_i - E_{nmda}) \qquad (3)$$

In which V is the membrane potential and E_{nmda} the reversal potential of the NMDA receptors. The term g_{nmda} is controlled by the pre-synaptic activity through P_{nmda} and the NMDA receptor Mg^{2+} block through $\widetilde{G}$. The NMDA receptor conductance g_{nmda} is thus given as:

$$g_{nmda} = \bar{g}_{nmda} P_{nmda} \widetilde{G} \qquad (4)$$

The term P_{nmda} represents the probability of glutamate binding to the post-synaptic NMDA receptors or, assuming a large number of post-synaptic NMDA receptors, it is equivalent to the number of NMDA receptors to which glutamate is bound. The term P_{nmda} is the product of two dynamical terms P^+ and P^- accounting for the fast rise ($\tau^+ = 1.5ms$) and slow decay ($\tau^- = 152ms$), respectively. Using the product of a fast and slow variable is equivalent to using a difference of exponentials, which is used to approach the activation of more detailed kinetic models of synaptic transmission (see Appendix C). The fast and slow variables are governed by:

$$\frac{dP^+}{dt} = \frac{1 - P^+}{\tau^+} + \delta_{pre}\alpha^+ P^+, \qquad (5)$$

$$\frac{dP^-}{dt} = \frac{0 - P^-}{\tau^-} + \delta_{pre}\alpha^-(1 - P^-) \qquad (6)$$

In which $\delta_{pre} = 1$ at the time of a pre-synaptic spike and $\delta_{pre} = 0$ otherwise. The terms α^+ and α^- determine the jump made in response to pre-synaptic activity and are equivalent to the amount of neurotransmitter release.

The NMDA receptors are blocked by Mg^{2+} at low membrane potentials, thus the NMDA receptor conductance g_{nmda} also depends on the voltage dependent unblocking (Jahr and Stevens 1990). Here the effect of the Mg^{2+} block is given by the function $G(V)$ (adapted from Dayan and Abbott 2001):

$$G(V) = \left(1 + \frac{[Mg^{2+}]}{3.56}exp[-V/16.12]\right)^{-1} \qquad (7)$$

Equation (7) calculates the Mg^{2+} block instantaneously, however it has been found that this is a non-instantaneous process (Kampa et al. 2004; Qian et al. 2005; Clarke and Johnson 2006). To account for the non-instantaneous blocking/unblocking a low-pass filtered version $\widetilde{G}$ is used, that follows the differential equation:

$$\tau_G \frac{d\widetilde{G}}{dt} = -\widetilde{G} + G(V_i) \qquad (8)$$

With τ_G as the time constant. The filter time constant τ_G is the second parameter which can be used to alter the specific shape of the STDP curve. The interpretation of changes in this variable is less clear than that of the low-pass filter time constant of the membrane potential τ_V, but it is related to different speeds of opening of the NMDA receptors. A possible underlying cause can be the different Mg^{2+} unblocking speeds of which some variability has been found (Vargas-Caballero and Robinson 2003; Kampa et al. 2004). Differences in channel subunit make-up can result in different Mg^{2+} unblocking time-courses (Vargas-Caballero and Robinson 2003; Qian et al. 2005; Clarke and Johnson 2006), but further investigation is needed to determine the factors that lead to differences captured by this parameter. Appendix D compares the NMDA receptor opening as used in this paper with the state model provided by Kampa et al. (2004). As will be shown later, for most STDP shapes this parameter is unchanged and only varied little when necessary.

The calcium concentration is then given by:

$$\frac{d[Ca^{2+}]}{dt} = \frac{(1 - [Ca^{2+}]) - \alpha I_{Ca^{2+}}^{(i)}}{\tau_{[Ca^{2+}]}} \tag{9}$$

This equation could possibly be extended to a case in which interactions between multiple proximal synapses are considered by some weighted summation of the independent calcium concentrations. The value for the time-constant $\tau_{[Ca^{2+}]}$ used in this paper (see Table 2) is larger than found by Sabatini et al. (2002), yet is of the order of magnitude reported by Markram et al. (1995) and of the NMDA receptor mediated EPSC reported by Lester et al. (1990). This leads to the possibility that the $[Ca^{2+}]$, governed by Eq. (9), does not purely represent the calcium concentration, but some slower process, dependent on the calcium concentration that saturises the calcium influx $I_{Ca^{2+}}$.

2.2 AMPA receptors

The modulation of the number and efficacy of AMPARs is thought to underlie the observed plasticity at these synapses (Malinow and Malenka 2002; Malenka and Bear 2004; Graupner and Brunel 2007). The phenomenological variable w_i captures the synaptic strength of synapse i. The AMPAR conductance g_{ampa} is given by:

$$g_{ampa} = w_i \bar{g}_{ampa} P_{ampa} \tag{10}$$

In which the interpretation of P_{ampa} is the same as P_{nmda} as used in the calculation of the NMDA receptor conductance (4), but then for the AMPARs. It follows the same dynamical equation as P^- in Eq. (6), but with a time constant of $\tau_{ampa} = 5.26ms$.

2.3 Synaptic plasticity

Departing from the observation that it is debatable whether only the magnitude of the $[Ca^{2+}]$ transients determine the direction of synaptic change, but that the specific evolution of the course is of importance (Sjöström and Nelson 2002; Rubin et al. 2005; Nevian and Sakmann 2006; Graupner and Brunel 2010) and that models using only the peak or average $[Ca^{2+}]$ levels have problems in reproducing classic STDP curves (Shouval and Kalantzis 2005; Gerkin et al. 2010), the changes in w_i will be governed by both the magnitude and time evolution of the Ca^{2+} current. The synaptic weight changes are calculated from two signals that are derived from the NMDA receptor-dependent Ca^{2+} current $I_{Ca^{2+}}$: a fast signal A_f which will determine the main shape of the STDP window and a slow signal A_s that will center the STDP curve around zero:

$$\Delta w_i = A_f \Theta(|A_f| - \varphi_f) - \alpha_s A_s \Theta(A_s - \varphi_s) \tag{11}$$

Where $\Theta(\cdot)$ is the Heaviside step function and φ_f and φ_s are thresholds to ensure that below a certain level no synaptic changes occur. The scaling factor α_s determines the amount in which A_s influences the resultant synaptic change, in effect it determines to what extend the STDP window is shifted downwards. The weight update of Eq. (11) may seem rather un-biophysical, considering existing models. However the aim of the current study is to propose a STDP mechanism that does not depend on the Ca^{2+} concentration, but rather takes experimental observations into account that show the importance of the dynamics of the Ca^{2+} current. Therefore we propose a signal that is derived from the Ca^{2+} dynamics, is consistent with experimental data, and results in the same synaptic changes.

The difference in time scale of the two signals is motivated by the observation that spike-timing-dependent LTP involves fast signalling and spike-timing-dependent LTD depends on a slower timescale (Yang et al. 1999; Gerkin et al. 2007). Additionally, a differential effect of fast and slow $[Ca^{2+}]$ rise on calmodulin has been found, resulting in potentiation and depression, respectively (DeMaria et al. 2001).

The slow signal A_s can be seen as the $[Ca^{2+}]$ in the spine that remains after the initial transient and is thus directly derived from the Ca^{2+} current $I_{Ca^{2+}}$:

$$\tau_s \frac{dA_s}{dt} = -A_s - (1 - A_s)I_{Ca^{2+}} \tag{12}$$

The signal A_s evolves with a relatively slow time constant $\tau_s \approx 8ms$ and its peak is therefore attenuated, this, combined with the thresholding function of the Heaviside step function, makes that this signal acts to induce LTD for Ca^{2+} levels above a certain threshold φ_s, similar to the LTD part of the calcium control models (Section 1.2).

Equation (12) includes a saturation which does not qualitatively alter the results of the current simulation (see Appendix B for a comparison of the simulation with and without this saturation). However it is thinkable that there are maximal bounds to the signals governing the synaptic change, therefore a saturation is included in the equation governing the evolution of the A_s signal.

The main determinant for the shape of the STDP curve is the fast signal A_f, which acts on a time scale of $\tau_f \approx 3.5ms$. The aim was to make the synaptic change dependent on other factors than the peak or average $[Ca^{2+}]$ alone, by taking into account a term that depends on the time course of the Ca^{2+} influx. As a simple initial approximation the first time-difference of the Ca^{2+} current is taken: $h\Delta I_{Ca^{2+}} = I_{Ca^{2+}}(t) - I_{Ca^{2+}}(t-h)$, with h being the simulation timestep. The signal A_f then follows:

$$\tau_f \frac{dA_f}{dt} = -A_f + \alpha_{A_f}(1 - A_f)\Delta I_{Ca^{2+}} \tag{13}$$

Also Eq. (13) includes a saturation, limiting the maximal value of the A_f signal. As opposed to the saturation in A_s (12), this saturation has a strong effect on the resulting synaptic change (see Appendix B). The fast signal A_f, and with that the gross shape of the STDP curve, depends effectively on a low-pass filtered version, with a non-linearity due to the saturation, of the rate of change of Ca^{2+} influx.

For the sake of simplicity, and because the weight changes in this study follow from abstract variables, we have omitted units where they are not crucial to the understanding of the proposed mechanisms.

## 3 Results

3.1 Calcium signals

In the proposed model the time-course of the Ca^{2+} current is the main factor determining the direction of the synaptic plasticity. The first models for Ca^{2+}-influx mediated plasticity relied on the peak or average $[Ca^{2+}]$ level to determine the sign of the synaptic change (Shouval et al. 2002; Abarbanel et al. 2003; Cai et al. 2007). Yet the $[Ca^{2+}]$ courses that result from *pre-post* and *post-pre* pairings, leading to LTP and LTD respectively, cannot be readily distinguished from one another (Nevian and Sakmann 2006; Graupner and Brunel 2010). Indeed, in the model developed in the current paper the $[Ca^{2+}]$ curves resulting from a *pre-post* (top panel) or a *post-pre* (bottom panel) pairing, shown in Fig. 3, do not differ from each other.

The specific time-courses of Ca^{2+} current do differ between the *pre-post* (top panel) and *post-pre* (bottom panel) pairings, as seen in Fig. 4. This supports the

Fig. 3 Ca^{2+} concentration timecourses for pre-before-post firing (top panel, $\Delta t = -20ms$) and post-before-pre firing (bottom panel, $\Delta t = 20ms$), leading to LTP and LTD respectively. Arrow indicates post-synaptic spike time; vertical line indicates pre-synaptic spike time
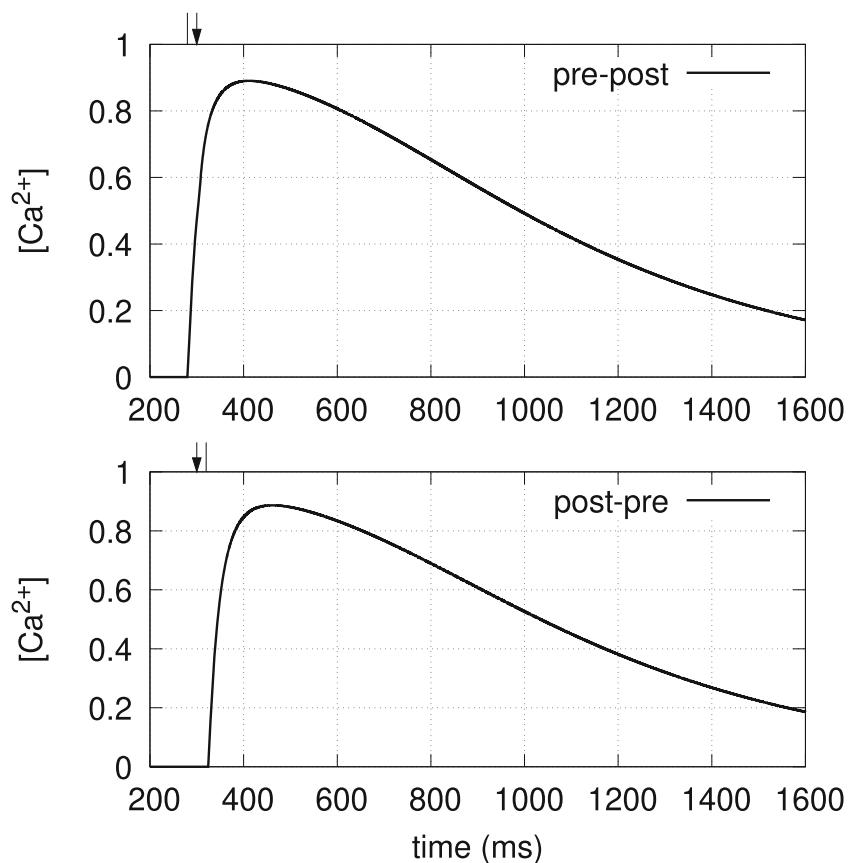
Fig. 4 Ca^{2+} current timecourses for pre-before-post firing (top panel, $\Delta t = -20ms$) and post-before-pre firing (bottom panel, $\Delta t = 20ms$), leading to LTP and LTD respectively. Arrow indicates post-synaptic spike time; vertical line indicates pre-synaptic spike time
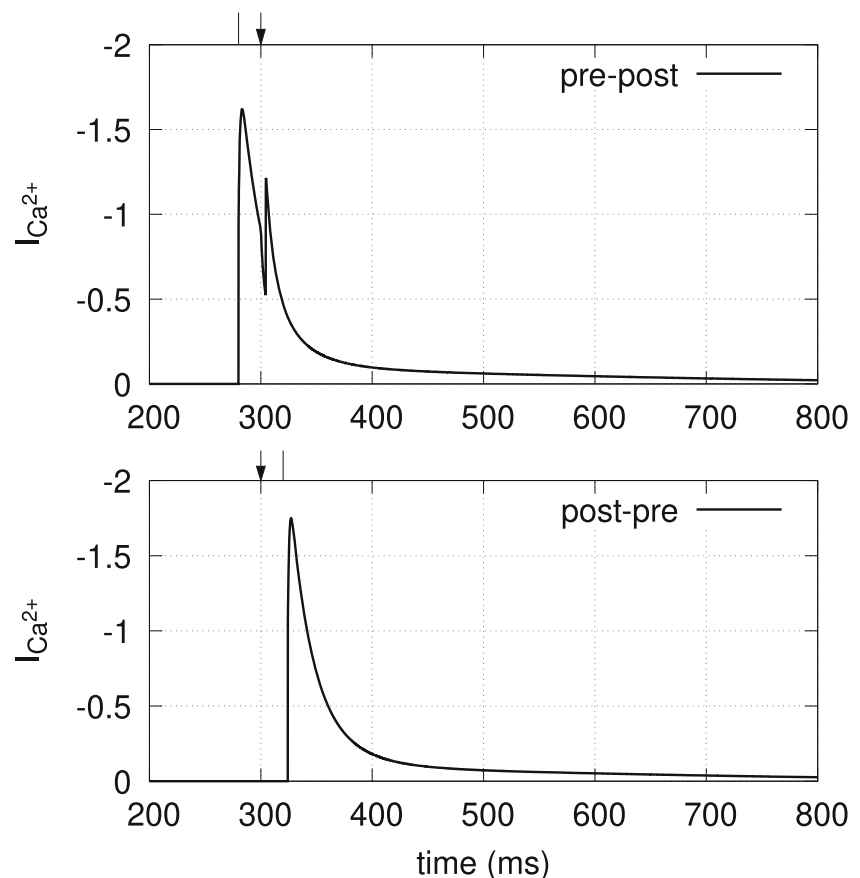
hypothesis of later models, which take the time-course of the Ca^{2+} influx into account (Rubin et al. 2005; Graupner and Brunel 2007; Urakubo et al. 2008; Gerkin et al. 2010). Opening the possibility for different timescales for LTP and LTD (Yang et al. 1999; Gerkin et al. 2007).

Figure 5 shows the fast A_f (black lines) and slow A_s (grey lines) signals, which determine the synaptic change for *pre-post* and *post-pre* pairings.

The fast signal A_f determines the sign and magnitude of the synaptic change. The sign is determined by the sign of the change in the Ca^{2+} current. A *pre-post* pairing will have two rising phases, one resulting from the release of neurotransmitter and a second due to the post-synaptic spike (see Fig. 4). Because the Ca^{2+} current $I_{Ca^{2+}}$ is influenced by the NMDA receptor conductance and attenuated by the internal Ca^{2+} concentration of the post-synaptic cell, the second peak in $I_{Ca^{2+}}$ is smaller than the initial rise in $I_{Ca^{2+}}$. Each rise in the A_f signal shows a large peak and a smaller, but wider, trough which, if this happens in isolation, as with a *post-pre* pairing, in effect results in LTD. Yet, if a *pre-post* pairing occurs, the A_f signal shows two peaks, which in effect leads to a LTP (see Fig. 5, black lines). Large increases in $I_{Ca^{2+}}$ and consequent, large enough amplitude fluctuations in A_f only occur when pre- and post-synaptic

activity occur within a certain time window. Isolated pre-synaptic activity leads only to small fluctuations, which cancel each other out. Isolated post-synaptic activity does not lead to LTP or LTD, because no Ca^{2+} current is evoked. The slow signal A_s mainly ensures that the STDP curve is centered around 0, with *pre-post* pairing leading to LTP and *post-pre* pairing leading to LTD, the courses of A_s do not differ greatly between *pre-post* and *post-pre* pairings (see Fig. 5). Isolated pre-synaptic activity leads to gradual increase in A_s, which eventually results in small LTD.

3.2 Classical & triplet STDP

The classic STDP induction protocol consists of repetitive pairing of pre-synaptic and post-synaptic activity with a certain time interval $\Delta t = t_{pre} - t_{post}$ between them. Repetitive pairing of pre-synaptic followed by post-synaptic activity ($\Delta t \leq 0$) results in LTP, whereas post-synaptic activity followed by pre-synaptic activity ($\Delta t > 0$) leads to LTD (Bi and Poo 1998; Abbott and Nelson 2000; Song et al. 2000). Figure 6 shows the result of single *pre-post* pairings at different Δt of the model (in grey) and the hypothetical curve (in black) as in phenomenological STDP models (Song et al. 2000). It shows a LTP window for

Fig. 5 Fast (black lines) and slow (grey lines) plasticity signals, again shown for *pre-post* firing (top panel, $\Delta t = -20ms$) and *post-pre* firing (bottom panel, $\Delta t = 20ms$), leading to LTP and LTD respectively. Arrow indicates post-synaptic spike time; vertical line indicates pre-synaptic spike time. The value for φ_s is indicated by the horizontal dashed line. The values φ_f is not shown, as it is set very close to zero
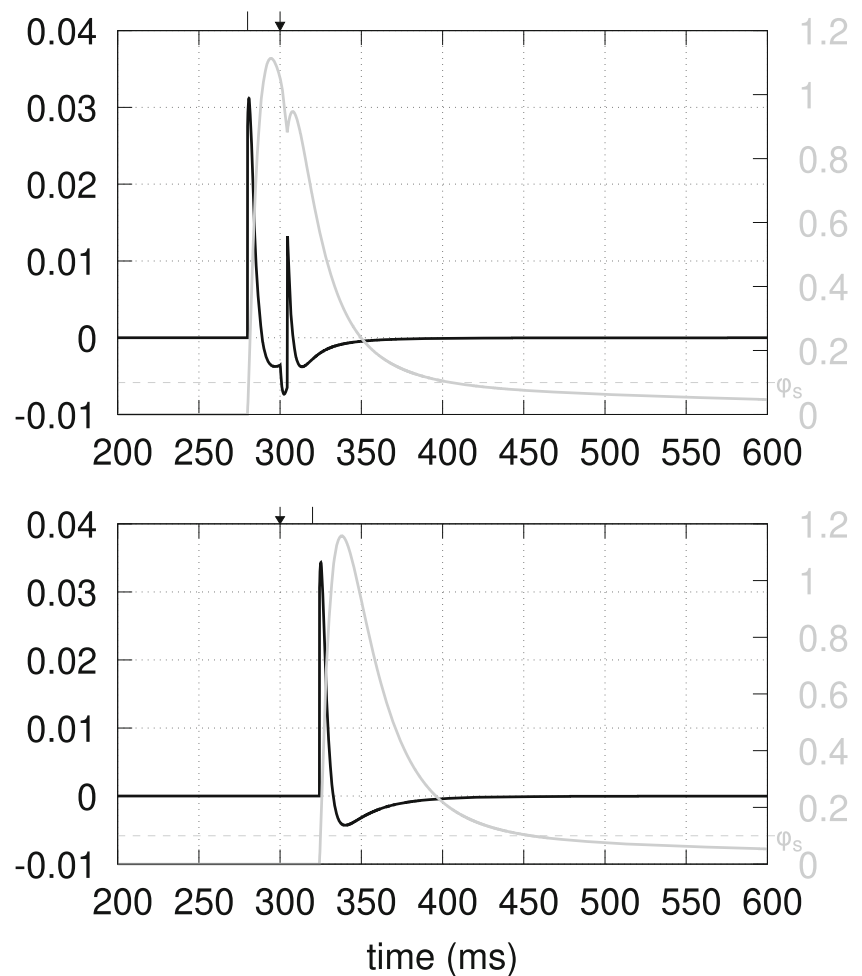

$-60ms < \Delta t \leq 0ms$ and a LTD window for $0ms < \Delta t < 50ms$.

The results of the classical STDP stimulation protocol thus result from the combination of the fast A_f and slow A_s signal, using Eq. (11). Figure 7 shows the synaptic change Δw (black lines) and the cumulative synaptic change (grey lines) per time step for two relative spike timings. The instantaneous synaptic change Δw is in big terms determined by the fast signal A_f, the slow signal A_s serves mainly to adjust the baseline for synaptic change.

Fig. 6 Classical STDP window resulting from the simulation of the classical STDP induction protocol with the proposed model. The figure shows the theoretical curve (thin black line) and the results of the model (grey thick line)
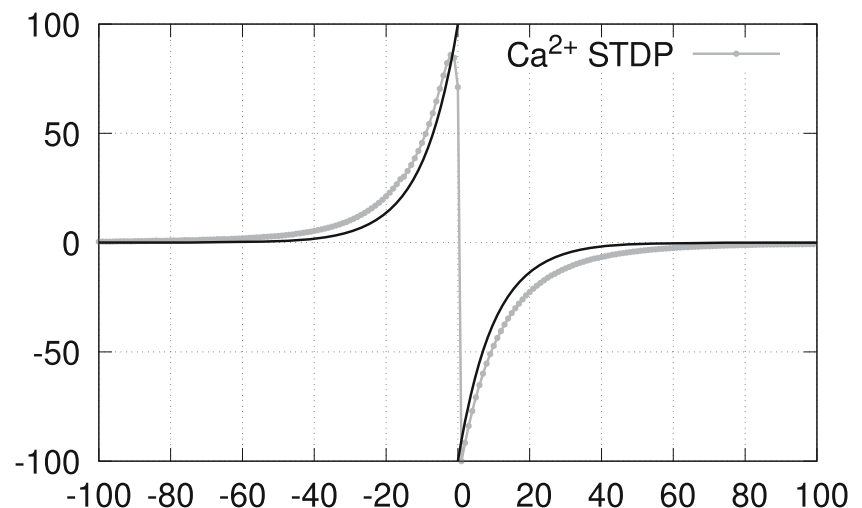
Fig. 7 Synaptic change versus time for *pre-post* firing (top panel, $\Delta t = -20ms$) and *post-pre* firing (bottom panel, $\Delta t = 20ms$), leading to LTP and LTD respectively. Synaptic change Δw is shown in black, using the left-hand axis. Cumulative synaptic change is in grey, using the right-hand axis. Insets give a closeup view of the cumulative synaptic change for the latter part of the simulation time (from $t = 500ms$ untill $t = 1000ms$). Arrow indicated post-synaptic spike time; vertical line indicates pre-synaptic spike time
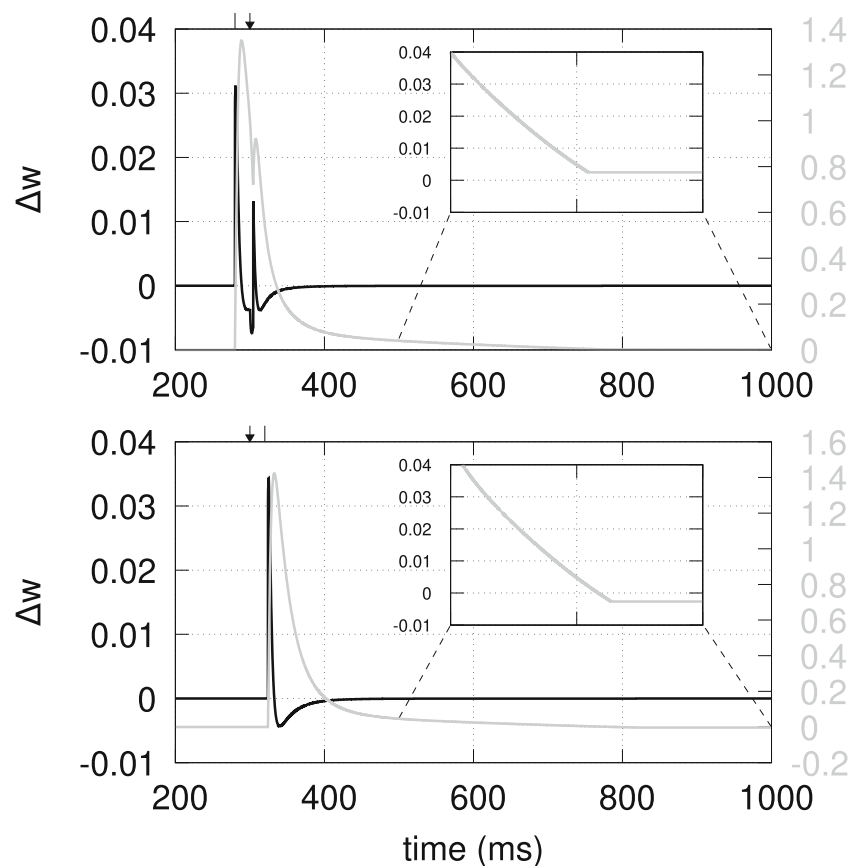

This figure shows that following the pre-synaptic spike (at time $t = 280ms$ in the top panel, and time $t = 320ms$ in the botom panel) the synaptic change rapidly makes a positive excursion, leading to a potentiation. However the longer negative trough and slow recovery of the instantaneous synaptic change Δw results in a rapid decrease of the cumulative synaptic change. In the case of *post-pre* firing (bottom panel) the post-synaptic activity (at $t = 300ms$, indicated by the arrow) occurs before any neurotransmitter is released in the synaptic cleft, only after the pre-synaptic spike (at $t = 320ms$, indicated by the vertical line), a synaptic change occurs. Due to this a single positive spike in the instantaneous synaptic change occurs, followed by a wider negative dip. The instantaneous synaptic change is negative for sufficiently long that it results in an overall negative synaptic change, or LTD. In case of *pre-post* firing (top panel) the pre-synaptic spike (at $t = 280ms$, indicated by the vertical line) results in an up-swing of the instantaneous synaptic change, due to the fact that the NMDA receptor block is never complete. The occurence of the post-synaptic spike (at $t = 300ms$, indicated by the arrow) results in another upsurge in the instantaneous synaptic change signal. This pushes up the cumulative synaptic change and results in a netto positive synaptic change, or LTP. The resulting synaptic changes are of a

small magnitide compared to the large excursion initially made by the cumulative synaptic change. The final synaptic change in these two cases is shown in the insets in Fig. 7.

3.2.1 Triplet STDP

Following the initial description of the STDP plasticity rule, it has been extended to spike-timing protocols with more than two spikes. In this it has been found that, instead of a linear summation of the STDP effects of individual spike pairs, the synaptic change follows from a more complex interaction between the spikes. For induction protocols with either one pre-synaptic spike and two post-synaptic spikes (*1 pre - 2 post*) or two pre-synaptic and one post-synaptic spike (*2 pre - 1 post*) it has been found that the sign of synaptic change is largely determined by the first two spikes (Froemke and Dan 2002; Froemke et al. 2006; Pfister and Gerstner 2006).

Figure 8 shows the synaptic changes resulting from triplets of spikes in which either one pre-synaptic spike is paired with two post-synaptic spikes (*1 pre - 2 post*, left column) or two pre-synaptic spikes are paired with one post-synaptic spike (*2 pre - 1 post*, right column). The values on the *x* and *y* axes indicate the difference in spike timing. For the *1 pre - 2 post* triplets, the *x* axis indicates

1 pre - 2 post

2 pre - 1 post

(a) linear summation

(b) linear summation
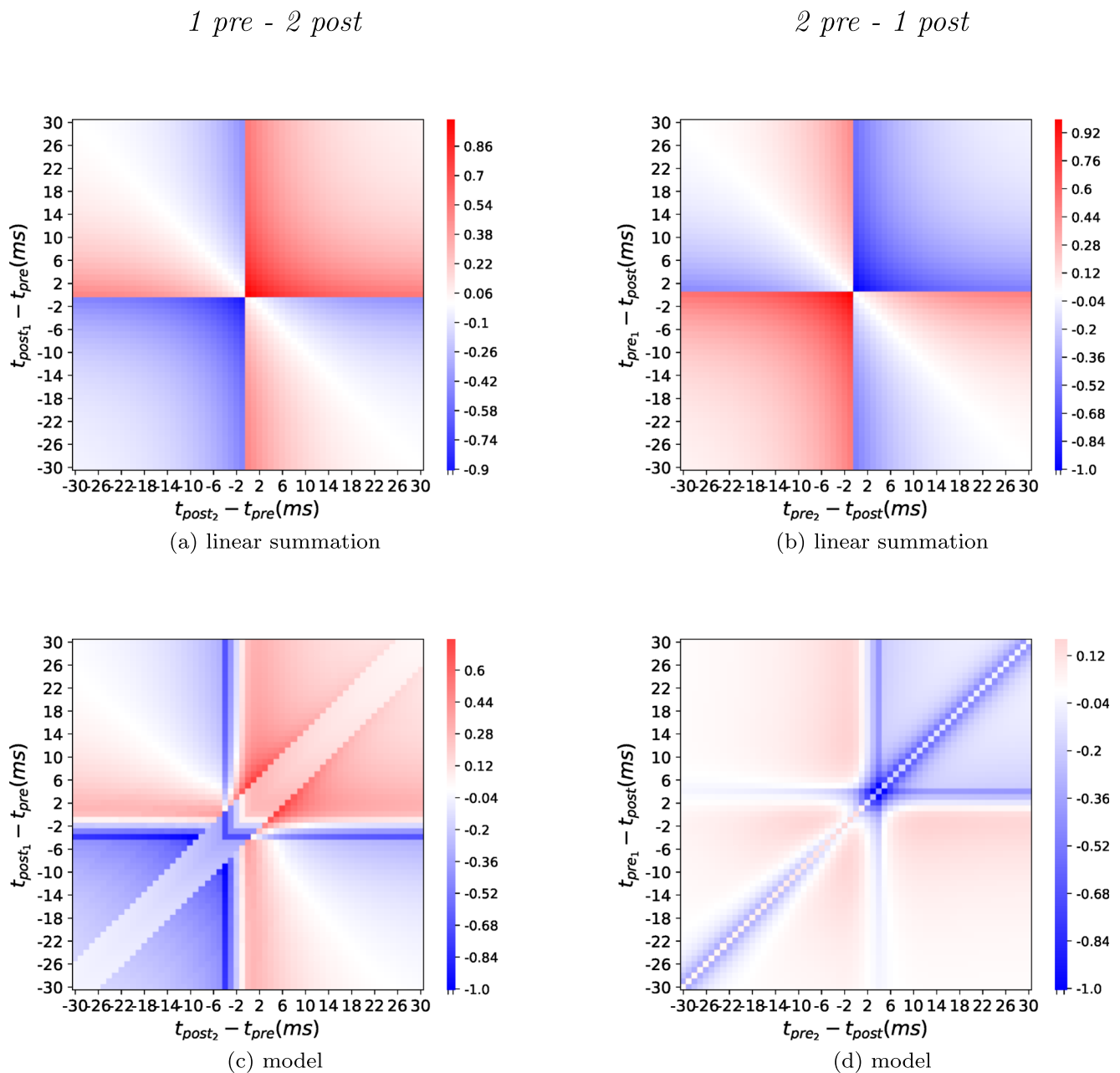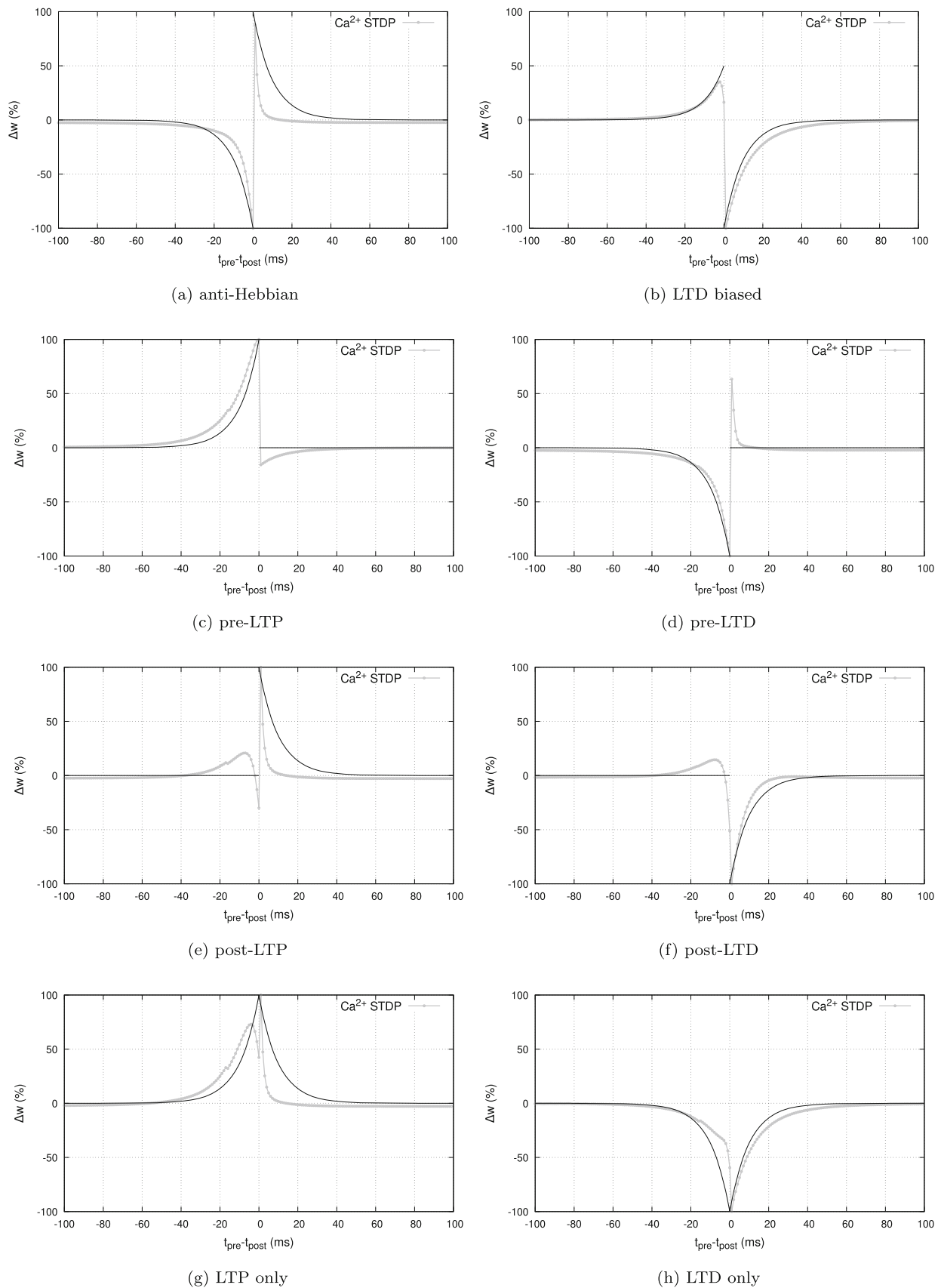

(c) model

(d) model

Fig. 8 Triplet STDP results of the proposed model. In all figures blue corresponds to LTD and red to LTP. The x- and y-axes denote the relative timing between the two post-synaptic and the single pre-synaptic spike in the left column, and the two pre-synaptic spikes and the single post-synaptic spike in the right column. **a** & **b** theoretical result following linear summation of the classical STDP model (Song et al. 2000); **c** & **d** results of the model for the triplet STDP induction protocol

the spike timing of one post-synaptic spike with respect to the pre-synaptic spike ($\Delta t_1 = t_{post}^{(1)} - t_{pre}$) and the y axis indicates the difference in spike timing between the other post-synaptic spike and the pre-synaptic spike ($\Delta t_2 = t_{post}^{(2)} - t_{pre}$). For the *2 pre - 1 post* triplets $\Delta t_1 = t_{pre}^{(1)} - t_{post}$ and $\Delta t_2 = t_{pre}^{(2)} - t_{post}$. Figure 8a and b show the effect of linear summation of triplets of spikes, in which in the areas in which the spikes alternate (either *post-pre-post* or *pre-post-pre* triplets) show LTP (in red) or LTD (in

blue) depending on the shortest spike-timing difference (see upper left and lower right quadrants of the plots in Fig. 8). However it was found that in these situations the sign of the synaptic change is mostly determined by the first two spikes and thus *post-pre-post* triples should lead to LTD and *pre-post-pre* triples should lead to LTP (Froemke and Dan 2002; Froemke et al. 2006). Yet, when the first time difference Δt_1 is very large relative to Δt_2, the effect of the last spike becomes more prominent, leading to LTP for *post-pre-post*

Fig. 9 Multiple STDP curves resulting from the simulation of the classical STDP protocol using different model parameters as denoted in Table 1

triplets and LTD for *pre-post-pre* triplets (Froemke and Dan 2002). This effect is replicated by the model, as can be seen in Fig. 8c and d. An unexpected area of LTD appears in the lower-left quadrant of Fig. 8d, whereas the result should solely be LTP in this region. Closer inspection revealed that the resulting LTD occurs only in a small region because of the two pre-synaptic spikes occuring within a very small time-window. This results in one single spike in the fast and slow signals, A_f and A_s, respectively, due to their integration times. The effect of this, and the ensuing deeper trough, result to a netto LTD. It is likely this can be cured by using different parameter settings.

3.3 Different STDP curves

The presented model is capable of exhibiting different STDP curves, as found in synapses of different cells (Abbott and Nelson 2000; Tzounopoulos et al. 2004; Lu et al. 2007; Fino et al. 2008) and at different locations on the dendrites (Froemke et al. 2005; Letzkus et al. 2006; Sjöström and Häusser 2006). In the model two parameters τ_V and τ_G, which control the timescale of change in the local synaptic membrane potential and the NMDA receptor Mg^{2+} unblocking respectively, can be tuned to obtain different STDP curves. Setting $\tau_V > 1ms$ result in a low-pass filtering of the membrane potential, whereas $0ms < \tau_V < 1ms$ results in a high-pass filtering and amplification. The parameter τ_G only takes on values $\tau_G > 1ms$, which relate to different speeds of the Mg^{2+} unblocking/blocking dynamics. For most STDP curves the value of τ_G is the same. Figure 9 shows some of the different STDP curves that the model is capable of producing. Table 1 shows the values used for τ_V and τ_G.

Different synapses of one cell can be differentiated through these parameters, making it possible to some extend to mimic the effects of a more complex morphology on the plasticity at different synapses, which can have important computational implications (Feldman 2012).

Table 1 Parameter values for different STDP curves

	$\tau_V (ms)$	$\tau_G (ms)$
Classical	10/9	20
Anti-Hebbian	2	2
LTD biased	4/3	20
Pre-LTP	2/3	20
Pre-LTD	100	1
Post-LTP	4/3	2
Post-LTD	20	20
LTP only	9/8	2
LTD only	2.5	20

4 Discussion

In the present study a model of Ca^{2+} influx-dependent synaptic plasticity for single compartment neuron models, that conforms to the classical STDP experiments (Bi and Poo 1998; Song et al. 2000) and STDP experiments with triplets of spikes (Froemke and Dan 2002; Froemke et al. 2006), is presented and tested. Moreover, the presented model is capable of exhibiting multiple types of STDP, by the tuning of two parameters. In this way the effects of different neurons and morphologies can be approximated.

It has been shown that *pre-post* and *post-pre* pairings result in similar $[Ca^{2+}]$ levels in the model, as is consistent with experimental observations *in vitro* (Nevian and Sakmann 2006). In the model this is due to the slow dynamcis of the equation governing $[Ca^{2+}]$ (9). The model thus affirms the hypothesis that the specific time-course of the Ca^{2+} influx is important to determine the change in synaptic weight (Sjöström and Nelson 2002), which has been used in other models of Ca^{2+}-mediated synaptic plasticity (Rubin et al. 2005; Graupner and Brunel 2007; Urakubo et al. 2008; Gerkin et al. 2010).

The proposed model replicates the classical STDP curve (Song et al. 2000) with *pre-post* spiking leading to LTP and *post-pre* spiking leading to LTD, with a clear switch from LTP to LTD with $\Delta t \leq 0$ to $\Delta t > 0$. The model also replicates the STDP results when considering triplets of spikes, where interchanging patterns of either *pre-post-pre* or *post-pre-post* spiking lead to LTP or LTD, mainly depending on the first two spikes (Froemke and Dan 2002; Froemke et al. 2006; Pfister and Gerstner 2006). An unexpected LTD area is observed in the lower left quadrant of Fig. 8d, which results due to an interaction between the two pre-synaptic spikes.

4.1 Interpretation of the model mechanisms

The mechanisms proposed in this study are of an abstract nature, and as such do not directly translate to biophysical mechanisms or structures. Experimental evidence points to an interplay of several Ca^{2+}-influx derived signals (Malenka et al. 1988; Yang et al. 1999; Mizuno et al. 2001; Lisman et al. 2012; Sjöström and Nelson 2002; Colbran 2004; Rubin et al. 2005; Wang et al. 2005; Nevian and Sakmann 2006; Feldman 2012; Lisman 2017), which is reflected in models of Ca^{2+}-governed plasticity (Lisman 1989; Rubin et al. 2005; Graupner and Brunel 2007; Kubota and Kitajima 2008; Urakubo et al. 2008; Gerkin et al. 2010; Graupner and Brunel 2010). Most of these models use two or more signals, which reflect the $[Ca^{2+}]$ or Ca^{2+}-current filtered over different time-scales, to differentially account for LTP and LTD (Rubin et al.

2005; Urakubo et al. 2008; Gerkin et al. 2010; Graupner and Brunel 2010). The simulation developed in this study shows that the main shape of the STDP curve can be largely recovered from a single signal: the change of the Ca^{2+}-current. The mechanism proposed here basically consists of a high-pass filtering of the Ca^{2+}-current (13), aided by additional signals that take care of saturation (9) and baseline correction (12). Yet, within this system there are several abstract signals, which can be captured by either one or several biophysical mechanisms.

The success of the presented model in the replication of several STDP experiments indicates that there is imporant information in the specific time-course of the Ca^{2+}-influx for STDP induced synaptic plasticity, and warrants further investigation into the specific biophysical mechanisms that can translate the Ca^{2+}-influx time-course into synaptic changes.

4.2 Different spike-timing dependencies

The main addition of this model is that it is possible for the model to express different STDP curves by altering just two parameters. Different values for $\tau_V > 1ms$ can be interpreted as placing the synapse at different distances from the axon hillock, because the properties of the cell membrane result in an attenuation and temporal spreading of the backpropagating action potential with distance it traveled (Sjöström and Häusser 2006). In the model this leads to different effects on the relation between relative spike-timing and synaptic change. An interesting future direction would be to investigate the influence of the stimulation protocol on the shape of the STDP window, as observed by Sjöström and Häusser (2006).

Passive dendrites have a low-pass filtering effect on the backpropagating action potential, but some dendrites can also actively propagate backpropagating action potentials (Sourdet and Debanne 1999; London and Häusser 2005). For instance, in interneurons a distance dependent increment in the amplitude of the backpropagating action potential-evoked Ca^{2+} transients has been found (Rozsa et al. 2004) and in layer 5 pyramidal neurons the rapid action potential time-course as seen at the soma is preserved throughout the dendritic tree (Holthoff et al. 2010). Setting $0ms < \tau_V < 1ms$ results in a high-pass filtering of the backpropagating action potential, which can be interpreted as a form of active propagation and modulation of the action potential backpropagation.

The parameter of τ_G has a less clear interpretation, however it has been shown that there is some variance in the Mg^{2+} (un)blocking timescales (Kampa et al. 2004). There is, to the knowledge of the authors, no data relating the synaptic properties to the variance of the (un)blocking speed.

4.3 Future work

In the current model the parameters to change the STDP curve are coarse phenomenological approximations of the possible biological causes underlying them. The interpretation of τ_V is readily given by the properties of passive and active properties of dendrites, but the parameter τ_G is less clearly defined. For both τ_V and τ_G more investigation is needed to uncover the specific mechanisms underlying these effects on the Ca^{2+} transients.

STDP is only one of the many plasticity mechanisms thought to be at work in neural systems (Feldman 2012; Lisman 2017; Zenke et al. 2015), therefore it will be necessary to develop models that model the underlying mechanisms of these other types of plasticity, in order to gain a complete model of synaptic plasticity.

Compliance with Ethical Standards

Conflict of interests The authors declare that they have no conflict of interest

## Appendix A: Table of parameters & values used

Table 2 Parameters and their values used in the simulations used to make the figures in the main text

| Equation	Parameter	Value used
1	τ_m	$10ms$
	g_L	$1mS/mm^2$
	E_l	$-65mV$
	E_{ampa}	$60mV$
	E_{nmda}	$0mV$
4	$\bar{g}_{nmda}$	$0.01mS/mm^2$
5	τ^+	$1.5ms$
	α^+	0.5
6	τ^-	$152ms$
	α^-	0.5
7	Mg^{2+}	$1mM$
9	α	10
	$\tau_{[Ca^{2+}]}$	$530ms$
10	$\bar{g}_{ampa}$	$0.05mS/mm^2$
11	φ_f	$1e{-}5$
	φ_s	0.1
	α_s	$7.4e{-}6$
13	α_{Af}	0.1

Appendix B: Comparison of saturated and unsaturated equations

In this appendix the effects of adding or removing certain saturations of the proposed models are investigated. As visible
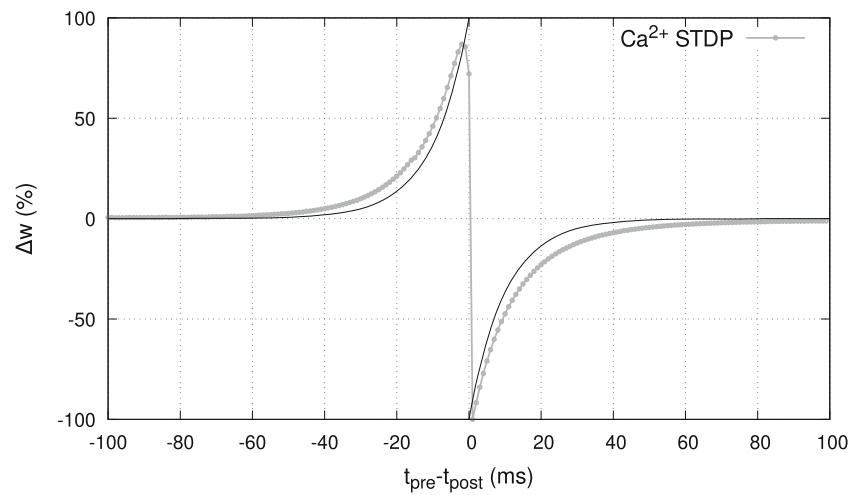
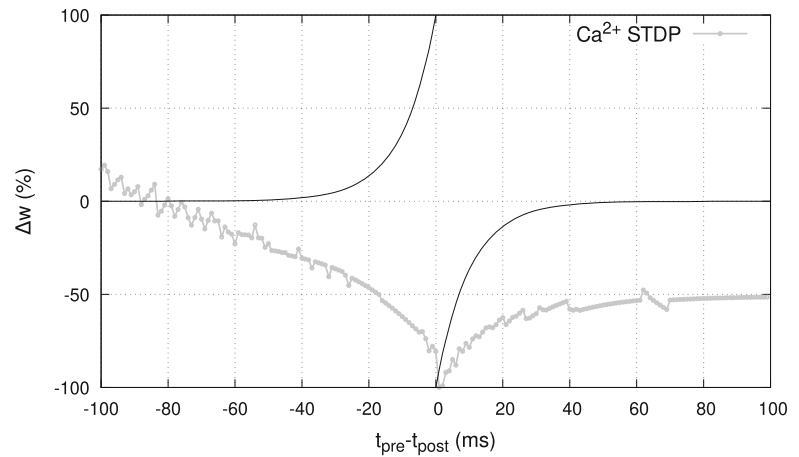**Fig. 10** Standard model, using the equations as stated in the main text
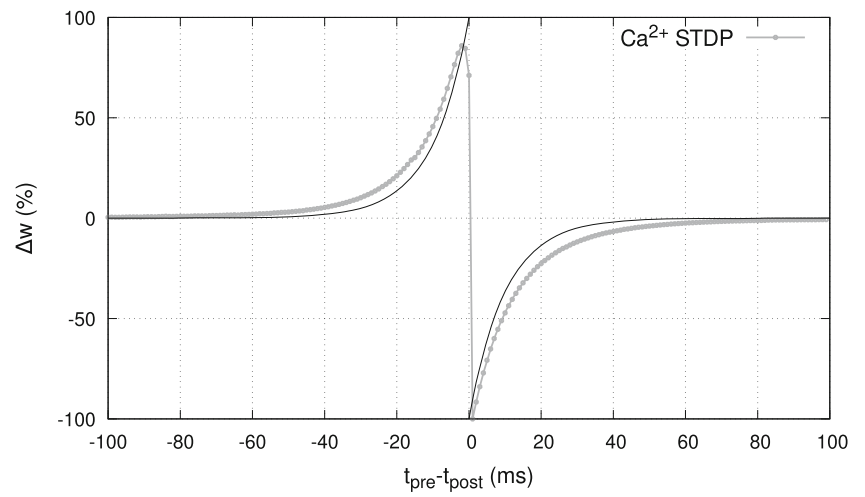
Fig. 11 Model with added saturation for $[Ca^{2+}]$. Parameters used: $\varphi_f = 2e{-}5$; $\varphi_s = 0.1$; $\alpha_s = 1.73e{-}5$
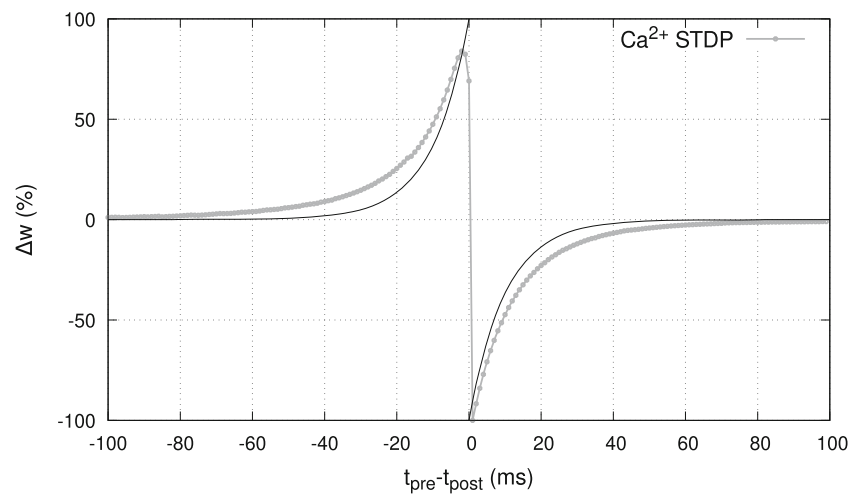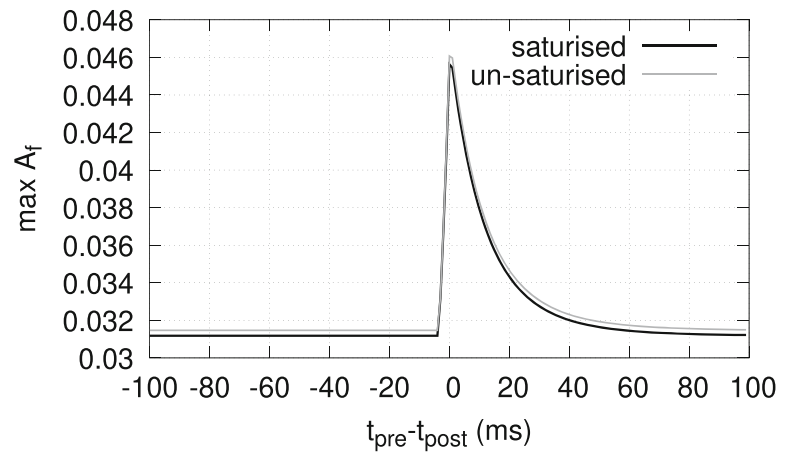

Fig. 12 Model with added saturation for A_s. Parameters used: $\varphi_f = 1e{-}5$; $\varphi_s = 0.05$; $\alpha_s = 9.5e{-}6$
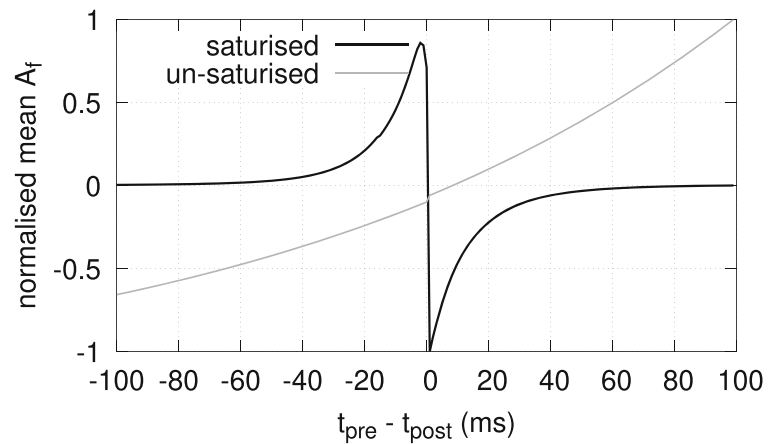
Fig. 13 Model with saturation removed for A_f. Same parameters as in main text

(a) resulting STDP window

(b) maximum A_f levels for different relative spike-timings. The black line corresponds to the saturised model, the grey line to the unsaturised model

(c) normalised mean A_f levels for different relative spike-timings. The black line corresponds to the saturised model, the grey line to the unsaturised model

in Figs. 11 and 12 the removal of the saturations of Eq. (9) and (12), respectively, does not affect the results in a qualitative manner. The absolute values of the resulting A_f and A_s signals differ, but the relative values between the different spike timings stay preserved as in the case of the main text (Fig. 10).
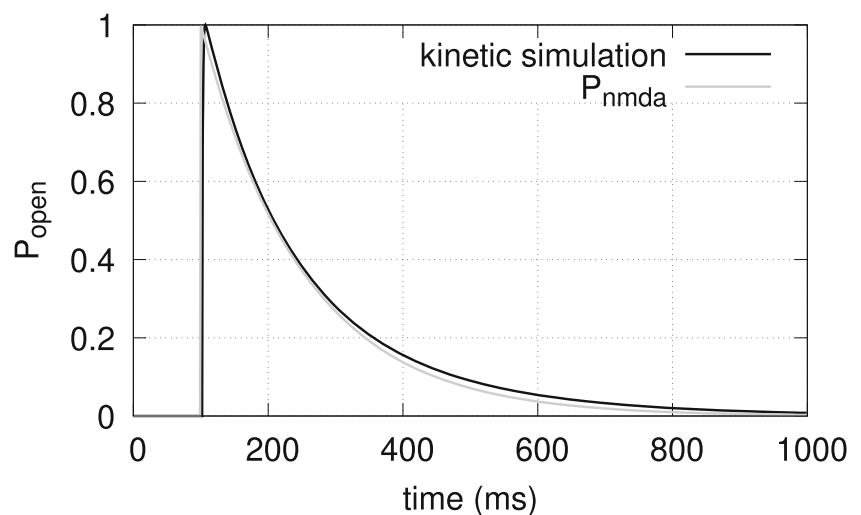
However removing the saturation in Eq. (13) leads to qualitatively different results, as shown in Fig. 13a. After inspection it was found that the main difference between the saturised and un-saturised model are the maximal and mean levels reached by the A_f signal for different relative spike timings. Figure 13b shows the maximal levels of the A_f signal for different spike timings and shows that the un-saturised model (grey line) has higher maximal values especially for large spiking intervals than the saturised model (black line). The values of the normalised mean A_f values, as shown in Fig. 13c, show that in the saturised model (black line) the basic shape of the STDP window is shown by the mean A_f values, whereas the un-saturised model (grey line) shows a very different shape.

Appendix C: Equivalence of NMDA receptor product and difference of exponentials models

In the main text the variable governing the open-probability of the post-synaptic NMDA receptors is modelled as a product of a slow and a fast variable (see Eqs. (5) & (6)). More conventionally, a difference of exponentials is used to model the NMDA receptor open probability, which is fitted to follow the opening probability of kinetic synaptic transmission models as proposed by Destexhe et al. (1994a, b, 1998). The difference of exponentials, as used by Dayan and Abbott (2001), is given as:

$$P_s = P_{max} B \left(e^{-t/\tau_1} - e^{-t/\tau_2} \right) \tag{14}$$

in which B is a normalising factor and $\tau_1 > \tau_2$ are time constants. The rise time of the variable P_s is given by: $\tau_{rise} = \frac{\tau_1 \tau_2}{\tau_1 - \tau_2}$ and the decay time is given by τ_1.

The variable used in this article is the product of a slow and a fast variable $P_{nmda} = P^+ P^-$. P^+ and P^- are governed by the differential equations (5) and (6), respectively. Integrating these equations, assuming a pre-synaptic pulse at time $t = 0$ gives:

$$P^+ = 1 - e^{-t/\tau^+} \quad \text{and} \quad P^- = e^{-t/\tau^-} \tag{15}$$

Leading to:

$$P = P^- P^+ = e^{-t/\tau^-} (1 - e^{-t/\tau^+}) \tag{16}$$
$$= e^{-t/\tau^-} - e^{-t/\tau^-} e^{-t/\tau^+} \tag{17}$$
$$= e^{-t/\tau^-} - e^{-\frac{\tau^- + \tau^+}{\tau^- \tau^+} t} \tag{18}$$

Then, by using the parameters from the main text ($\tau^+ = 1.5ms$ and $\tau^- = 152ms$), one finds that the decay time of the difference of exponentials is $\tau_1 = \tau^- = 152ms$, and the rise time $\tau_{rise} \approx 1.5ms$. Thus it is shown that the product of a slow and fast variable and the difference of exponentials models for synaptic opening are equivalent in this case. Figure 14 compares the results of a numerical simulation of the kinetic scheme for the NMDA synaptic transmission, as described in Destexhe et al. (1998), with the model for P_{nmda} used in this manuscript (Eqs. (5) and (6)).

Appendix D: Comparison of NMDA receptor opening simulations

In the presented model the NMDA recptor opening g_{nmda} (4) is goverened by the NMDA receptor open probability P_{nmda} (Eqs. (5) and (6)), which is related to the binding of glutamate to the receptor, and the Mg^{2+} unblocking $\widetilde{G}$, which is modelled as a low-passed version of the direct

Fig. 14 Comparison of the numerical simulation of the kinetic model for NMDA synaptic transmission (black line) and the synaptic transmission model used in the proposed model (grey line) for a single pulse of neurotransmitter at $t = 100ms$

Fig. 15 Comparison of the kinetic model of NMDA receptor opening (black line) and the NMDA receptor opening used in the current paper (grey line) for a single pre-post pairing ($t_{pre} - t_{post} = -10ms$). In this simulation $\tau^+ = 2ms$ (5) and $\tau^- = 105ms$ (6). Pre-synaptic timing (glutamate release) is indicated by the vertical line. Post-synaptic activity occurs at the arrow
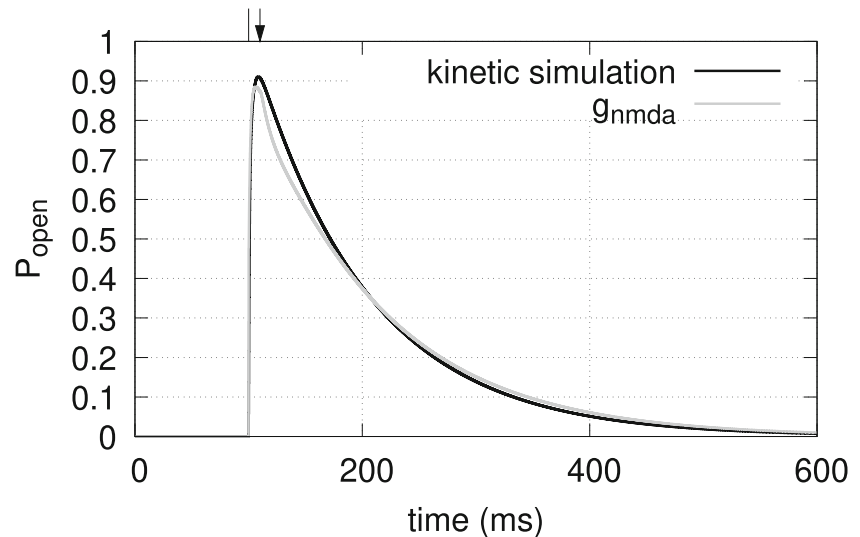

Mg^{2+} unblocking as given by Eq. (7) (Jahr and Stevens 1990; Dayan and Abbott 2001). Using a low-passed version of the Mg^{2+} unblocking is motivated by the observation that the unblock is not instantaneous (Vargas-Caballero and Robinson 2003; Kampa et al. 2004) and that the specific channel sub-unit make-up can alter the Mg^{2+} unblocking time-course (Vargas-Caballero and Robinson 2003; Qian et al. 2005; Clarke and Johnson 2006). In their paper, Kampa et al. (2004) provide a kinetic model that captures the non-instantaneous effect of the Mg^{2+} unblocking as they find in their data. This appendix provides a comparison between the kinetic model and Eqs. (4) through (8).

Simulations of both the kinetic model of Kampa et al. (2004) and Eqs. (4)–(8) have been done using one *pre-post* and one *post-pre* spike pairing, the same as during one run on the STDP induction protocol, with an inter-spike interval of $10ms$. Figure 15 shows the resulting NMDA receptor opening following a *pre-post* pairing, Fig. 16 shows the

NMDA receptor opening following a *post-pre* pairing. The black lines show the NMDA receptor opening as predicted by the Kampa et al. (2004) kinetic model, the NMDA receptor opening used in this paper is given by the grey lines. The P_{nmda} rise and fall time constants of Eqs. (5) and (6), respectively, have been altered in order to obtain a better fit with the kinetic model ($\tau^+ = 2ms$, $\tau^- = 105ms$).

The results show large agreement in NMDA receptor opening between the kinetic model and Eqs. (4)–(8). The opening time-courses in the *pre-post* spike pairing case, shown in Fig. 15, show that the model used in this paper follows a decay time-course with a slight change in the decay rate around $t \approx 120ms$ in Fig. 15, due to the different interacting terms that lead to the NMDA receptor opening. However the two methods are in agreement on the large-scale shape and magnitude of the NMDA receptor opening. Figure 16 shows the results of both methods following a *post-pre* spike pairing. The peak magnitude of the NMDA

Fig. 16 Comparison of the kinetic model of NMDA receptor opening (black line) and the NMDA receptor opening used in the current paper (solid line) for a single post-pre pairing ($t_{pre} - t_{post} = 10ms$). In this simulation $\tau^+ = 2ms$ (5) and $\tau^- = 105ms$ (6). Pre-synaptic timing (glutamate release) is indicated by the vertical line. Post-synaptic activity occurs at the arrow
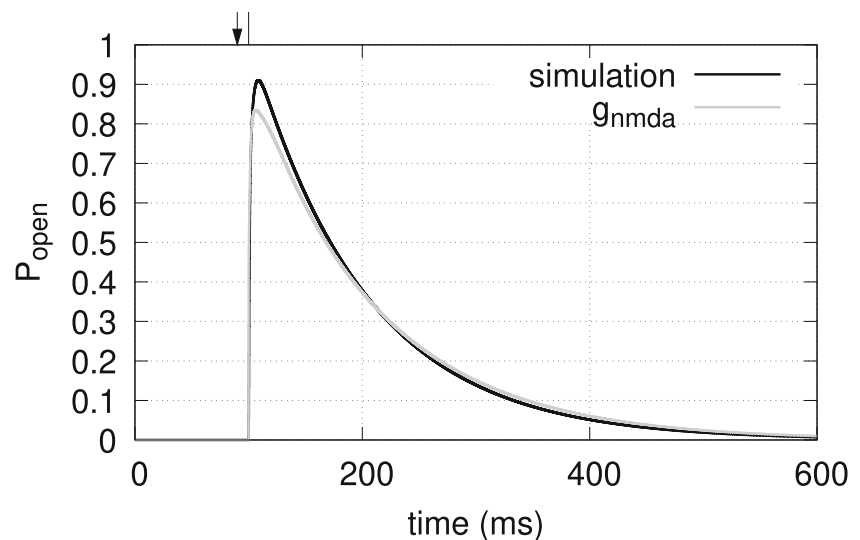
receptor opening given by Eqs. (4)–(8) is slightly lower than that of the kinetic model, however, the models agree on the large scale shape of the NMDA receptor opening time-course.

References

Abarbanel, H.D., Gibb, L., Huerta, R., Rabinovich, M.I. (2003). Biophysical model of synaptic plasticity dynamics. *Biological Cybernetics*, *89*(3), 214–226.

Abbott, L.F., & Nelson, S.B. (2000). Synaptic plasticity: taming the beast. *Nature Neuroscience*, *3*(11s), 1178.

Badoual, M., Zou, Q., Davison, A.P., Rudolph, M., Bal, T., Frégnac, Y., Destexhe, A. (2006). Biophysical and phenomenological models of multiple spike interactions in spike-timing dependent plasticity. *International Journal of Neural Systems*, *16*(02), 79–97.

Bi, G.-q., & Poo, M.-m. (1998). Synaptic modifications in cultured hippocampal neurons: dependence on spike timing, synaptic strength, and postsynaptic cell type. *Journal of Neuroscience*, *18*(24), 10464–10472.

Cai, Y., Gavornik, J.P., Cooper, L.N., Yeung, L.C., Shouval, H.Z. (2007). Effect of stochastic synaptic and dendritic dynamics on synaptic plasticity in visual cortex and hippocampus. *Journal of Neurophysiology*, *97*(1), 375–386.

Carlson, K.D., & Giordano, N. (2011). Interplay of the magnitude and time-course of postsynaptic ca 2+ concentration in producing spike timing-dependent plasticity. *Journal of Computational Neuroscience*, *30*(3), 747–758.

Clarke, R.J., & Johnson, J.W. (2006). Nmda receptor nr2 subunit dependence of the slow component of magnesium unblock. *Journal of Neuroscience*, *26*(21), 5825–5834.

Colbran, R.J. (2004). Protein phosphatases and calcium/calmodulin-dependent protein kinase II-dependent synaptic plasticity. *Journal of Neuroscience*, *24*(39), 8404–8409.

Dayan, P., & Abbott, L.F. (2001). *Theoretical neuroscience* Vol. 806. Cambridge: MIT Press.

DeMaria, C.D., Soong, T.W., Alseikhan, B.A., Alvania, R.S., Yue, D.T. (2001). Calmodulin bifurcates the local Ca2+ signal that modulates P/Q-type Ca2+ channels. *Nature*, *411*(6836), 484.

Destexhe, A., Mainen, Z.F., Sejnowski, T.J. (1994a). An efficient method for computing synaptic conductances based on a kinetic model of receptor binding. *Neural Computation*, *6*(1), 14–18.

Destexhe, A., Mainen, Z.F., Sejnowski, T.J. (1994b). Synthesis of models for excitable membranes, synaptic transmission and neuromodulation using a common kinetic formalism. *Journal of Computational Neuroscience*, *1*(3), 195–230.

Destexhe, A., Mainen, Z.F., Sejnowski, T.J. (1998). Kinetic models of synaptic transmission. *Methods in Neuronal Modeling*, *2*, 1–25.

Feldman, D.E. (2012). The spike-timing dependence of plasticity. *Neuron*, *75*(4), 556–571.

Fino, E., Deniau, J.-M., Venance, L. (2008). Cell-specific spike-timing-dependent plasticity in GABAergic and cholinergic interneurons in corticostriatal rat brain slices. *The Journal of Physiology*, *586*(1), 265–282.

Froemke, R.C., & Dan, Y. (2002). Spike-timing-dependent synaptic modification induced by natural spike trains. *Nature*, *416*(6879), 433.

Froemke, R.C., Poo, M.-m., Dan, Y. (2005). Spike-timing-dependent synaptic plasticity depends on dendritic location. *Nature*, *434*(7030), 221.

Froemke, R.C., Tsay, I.A., Raad, M., Long, J.D., Dan, Y. (2006). Contribution of individual spikes in burst-induced long-term synaptic modification. *Journal of Neurophysiology*, *95*(3), 1620–1629.

Gerkin, R.C., Lau, P.-M., Nauen, D.W., Wang, Y.T., Bi, G.-Q. (2007). Modular competition driven by NMDA receptor subtypes in spike-timing-dependent plasticity. *Journal of Neurophysiology*, *97*(4), 2851–2862.

Gerkin, R.C., Bi, G.-Q., Rubin, J.E. (2010). A phenomenological calcium-based model of STDP. In *Hippocampal microcircuits* (pp. 571–591): Springer.

Gerstner, W., Kempter, R., van Hemmen, J.L., Wagner, H. (1996). A neuronal learning rule for sub-millisecond temporal coding. *Nature*, *383*(6595), 76.

Graupner, M., & Brunel, N. (2007). STDP in a bistable synapse model based on CaMKII and associated signaling pathways. *PLoS Computational Biology*, *3*(11), e221.

Graupner, M., & Brunel, N. (2010). Mechanisms of induction and maintenance of spike-timing dependent plasticity in biophysical synapse models. *Frontiers in Computational Neuroscience*, *4*, 136.

Hebb, D. (1949). *The organization of behavior*. New York: Wiley.

Holmes, W.R. (2000). Models of calmodulin trapping and cam kinase ii activation in a dendritic spine. *Journal of Computational Neuroscience*, *8*(1), 65–86.

Holthoff, K., Zecevic, D., Konnerth, A. (2010). Rapid time course of action potentials in spines and remote dendrites of mouse visual cortex neurons. *The Journal of Physiology*, *588*(7), 1085–1096.

Jahr, C.E., & Stevens, C.F. (1990). Voltage dependence of NMDA-activated macroscopic conductances predicted by single-channel kinetics. *Journal of Neuroscience*, *10*(9), 3178–3182.

Kampa, B.M., Clements, J., Jonas, P., Stuart, G.J. (2004). Kinetics of Mg2+ unblock of NMDA receptors: implications for spike-timing dependent synaptic plasticity. *The Journal of Physiology*, *556*(2), 337–345.

Karmarkar, U.R., & Buonomano, D.V. (2002). A model of spike-timing dependent plasticity: one or two coincidence detectors? *Journal of Neurophysiology*, *88*(1), 507–513.

Kubota, S., & Kitajima, T. (2008). A model for synaptic development regulated by nmda receptor subunit expression. *Journal of Computational Neuroscience*, *24*(1), 1–20.

Lester, R.A., Clements, J.D., Westbrook, G.L., Jahr, C.E. (1990). Channel kinetics determine the time course of nmda receptor-mediated synaptic currents. *Nature*, *346*(6284), 565.

Letzkus, J.J., Kampa, B.M., Stuart, G.J. (2006). Learning rules for spike timing-dependent plasticity depend on dendritic synapse location. *Journal of Neuroscience*, *26*(41), 10420–10429.

Lisman, J. (1989). A mechanism for the Hebb and the anti-Hebb processes underlying learning and memory. *Proceedings of the National Academy of Sciences*, *86*(23), 9574–9578.

Lisman, J. (2017). Glutamatergic synapses are structurally and biochemically complex because of multiple plasticity processes: long-term potentiation, long-term depression, short-term potentiation and scaling. *Philosophical Transactions of the Royal Society B*, *372*(1715), 20160260.

Lisman, J., Yasuda, R., Raghavachari, S. (2012). Mechanisms of CaMKII action in long-term potentiation. *Nature Reviews Neuroscience*, *13*(3), 169.

London, M., & Häusser, M. (2005). Dendritic computation. *Annual Review of Neuroscience*, *28*, 503–532.

Lu, J.-t., Li, C.-y., Zhao, J.-P., Poo, M.-m., Zhang, X.-h. (2007). Spike-timing-dependent plasticity of neocortical excitatory synapses on inhibitory interneurons depends on target cell type. *Journal of Neuroscience*, *27*(36), 9711–9720.

Malenka, R.C., & Bear, M.F. (2004). LTP and LTD: an embarrassment of riches. *Neuron*, *44*(1), 5–21.

Malenka, R.C., Kauer, J.A., Perkel, D.J., Mauk, M.D., Kelly, P.T., Nicoll, R.A., Waxham, M.N. (1989). An essential role for postsynaptic calmodulin and protein kinase activity in long-term potentiation. *Nature*, *340*(6234), 554.

Malenka, R.C., Kauer, J.A., Zucker, R.S., Nicoll, R.A. (1988). Postsynaptic calcium is sufficient for potentiation of hippocampal synaptic transmission. *Science*, *242*(4875), 81–84.

Malinow, R., & Malenka, R.C. (2002). AMPA receptor trafficking and synaptic plasticity. *Annual Review of Neuroscience*, *25*(1), 103–126.

Markram, H., Helm, P.J., Sakmann, B. (1995). Dendritic calcium transients evoked by single back-propagating action potentials in rat neocortical pyramidal neurons. *The Journal of Physiology*, *485*(1), 1–20.

Markram, H., Lübke, J., Frotscher, M., Sakmann, B. (1997). Regulation of synaptic efficacy by coincidence of postsynaptic APs and EPSPs. *Science*, *275*(5297), 213–215.

Mizuno, T., Kanazawa, I., Sakurai, M. (2001). Differential induction of ltp and ltd is not determined solely by instantaneous calcium concentration: an essential involvement of a temporal factor. *European Journal of Neuroscience*, *14*(4), 701–708.

Nevian, T., & Sakmann, B. (2006). Spine Ca2+ signaling in spike-timing-dependent plasticity. *Journal of Neuroscience*, *26*(43), 11001–11013.

Pfister, J.-P., & Gerstner, W. (2006). Triplets of spikes in a model of spike timing-dependent plasticity. *Journal of Neuroscience*, *26*(38), 9673–9682.

Qian, A., Buller, A.L., Johnson, J.W. (2005). Nr2 subunit-dependence of nmda receptor channel block by external mg2+. *The Journal of Physiology*, *562*(2), 319–331.

Rozsa, B., Zelles, T., Vizi, E.S., Lendvai, B. (2004). Distance-dependent scaling of calcium transients evoked by backpropagating spikes and synaptic activity in dendrites of hippocampal interneurons. *Journal of Neuroscience*, *24*(3), 661–670.

Rubin, J.E., Gerkin, R.C., Bi, G.-Q., Chow, C.C. (2005). Calcium time course as a signal for spike-timing-dependent plasticity. *Journal of Neurophysiology*, *93*(5), 2600–2613.

Sabatini, B.L., Oertner, T.G., Svoboda, K. (2002). The life cycle of ca2+ ions in dendritic spines. *Neuron*, *33*(3), 439–452.

Shouval, H.Z., & Kalantzis, G. (2005). Stochastic properties of synaptic transmission affect the shape of spike time-dependent plasticity curves. *Journal of Neurophysiology*, *93*(2), 1069–1073.

Shouval, H.Z., Bear, M.F., Cooper, L.N. (2002). A unified model of NMDA receptor-dependent bidirectional synaptic plasticity.

Proceedings of the National Academy of Sciences, *99*(16), 10831–10836.

Sjöström, P.J., & Häusser, M. (2006). A cooperative switch determines the sign of synaptic plasticity in distal dendrites of neocortical pyramidal neurons. *Neuron*, *51*(2), 227–238.

Sjöström, P.J., & Nelson, S.B. (2002). Spike timing, calcium signals and synaptic plasticity. *Current Opinion in Neurobiology*, *12*(3), 305–314.

Song, S., Miller, K.D., Abbott, L.F. (2000). Competitive Hebbian learning through spike-timing-dependent synaptic plasticity. *Nature Neuroscience*, *3*(9), 919.

Sourdet, V., & Debanne, D. (1999). The role of dendritic filtering in associative long-term synaptic plasticity. *Learning & Memory*, *6*(5), 422–447.

Tzounopoulos, T., Kim, Y., Oertel, D., Trussell, L.O. (2004). Cell-specific, spike timing–dependent plasticities in the dorsal cochlear nucleus. *Nature Neuroscience*, *7*(7), 719.

Urakubo, H., Honda, M., Froemke, R.C., Kuroda, S. (2008). Requirement of an allosteric kinetics of NMDA receptors for spike timing-dependent plasticity. *Journal of Neuroscience*, *28*(13), 3310–3323.

Vargas-Caballero, M., & Robinson, H.P. (2003). A slow fraction of Mg2+ unblock of NMDA receptors limits their contribution to spike generation in cortical pyramidal neurons. *Journal of Neurophysiology*, *89*(5), 2778–2783.

Wang, H.-X., Gerkin, R.C., Nauen, D.W., Bi, G.-Q. (2005). Coactivation and timing-dependent integration of synaptic potentiation and depression. *Nature Neuroscience*, *8*(2), 187.

Waters, J., Schaefer, A., Sakmann, B. (2005). Backpropagating action potentials in neurones: measurement, mechanisms and potential functions. *Progress in Biophysics and Molecular Biology*, *87*(1), 145–170.

Yang, S.-N., Tang, Y.-G., Zucker, R.S. (1999). Selective induction of LTP and LTD by postsynaptic [Ca2+]i elevation. *Journal of Neurophysiology*, *81*(2), 781–787.

Zenke, F., Agnes, E.J., Gerstner, W. (2015). Diverse synaptic plasticity mechanisms orchestrated to form and retrieve memories in spiking neural networks. *Nature Communications*, *6*, 6922.